Rashba spin-orbit coupling in infinite-layer nickelate films on $SrTiO_3(001)$ and $KTaO_3(001)$

Benjamin Geisler*
Department of Physics, University of Florida, Gainesville, Florida 32611, USA
and Department of Materials Science and Engineering, University of Florida, Gainesville, Florida 32611, USA

(Received 1 February 2023; revised 7 October 2023; accepted 15 November 2023; published 1 December 2023)

The impact of spin-orbit interactions in $NdNiO_2/SrTiO_3(001)$ and $NdNiO_2/KTaO_3(001)$ is explored by performing density functional theory simulations including a Coulomb repulsion term. Polarity mismatch drives the emergence of an interfacial two-dimensional electron gas in $NdNiO_2/KTaO_3(001)$ involving the occupation of Ta $5d$ conduction-band states, which is twice as pronounced as in $NdNiO_2/SrTiO_3(001)$. We identify a significant anisotropic k^3 Rashba spin splitting of the respective d_{xy} states in both systems that results from the broken inversion symmetry at the nickelate-substrate interface and exceeds the width of the superconducting gap. In $NdNiO_2/KTaO_3(001)$, the splitting reaches 210 meV, which is comparable to Bi(111) surface states. At the surface, the Ni $3d_{x^2-y^2}$-derived states exhibit an unexpectedly strong linear Rashba effect with $\alpha_R \sim 125$ meV Å, exemplifying its orbital selectivity. The corresponding Fermi sheets present a reconstructed circular shape due to the electrostatic doping, but undergo a Lifshitz transition towards a cupratelike topology deeper in the film that coincides with a realignment of their spin texture. These results promote surface and interface polarity as interesting design parameters to control spin-orbit physics as well as the superconducting pairing in infinite-layer nickelate heterostructures.

DOI: 10.1103/PhysRevB.108.224502

I. INTRODUCTION

Spin-orbit coupling (SOC) correlates the electron spin and the crystal lattice and gives rise to a multitude of intriguing quantum phenomena. A prominent example is the Rashba effect [1], which originates from the broken inversion symmetry at interfaces and surfaces and is of fundamental relevance in spintronics, as it permits the electric control of the spin precession [2]. Moreover, it plays a key role in the quest to realize Majorana zero modes by exploiting the proximity effect between a material with strong SOC and a superconductor [3–5]. The pronounced coupling of lattice, orbital, spin, and charge degrees of freedom in transition metal oxides [6] renders them a particularly interesting platform to explore superconductivity in conjunction with a two-dimensional Rashba system. Paradigmatic is the $LaAlO_3/SrTiO_3(001)$ interface [7–11], where the Rashba effect is considered to stabilize the emergent superconducting phase [12–14] and may reconcile superconductivity and magnetism [15,16].

The very recent observation of superconductivity in Sr-doped $NdNiO_2$, $PrNiO_2$, and $LaNiO_2$ films grown on $SrTiO_3(001)$ (STO) [17–21] sparked considerable interest in $3d^9$ infinite-layer (ABO_2) nickelates, which are formally isoelectronic to the cuprates [22–44]. However, superconductivity remained elusive in the respective bulk compounds so far [45,46]. Early work unraveled the key role of the polar interface [47–51]: The polarity mismatch drives the formation of a two-dimensional electron gas (2DEG) in the substrate by occupation of the interfacial Ti $3d$ states [47,51] that is considerably more pronounced than in $LaAlO_3/STO(001)$ [10]. Therefore, these artificial oxides naturally host a 2DEG proximate to a novel class of superconductors.

An intriguing alternative to STO is $KTaO_3$ (KTO), which exhibits stronger spin-orbit interactions [52] and attracts increasing attention due to the emergence of superconductivity at different (111) and (110) heterointerfaces [53–55]. Moreover, 2DEGs have been reported in a variety of (001)-oriented perovskite systems [56–58].

Here we explore the impact of spin-orbit interactions in $NdNiO_2/STO(001)$ and $NdNiO_2/KTO(001)$ by performing density functional theory simulations including a Coulomb repulsion term in explicit film geometry. The distinct polar discontinuity at the $Nd^{3+}/(TiO_2)^0$ versus $Nd^{3+}/(TaO_2)^{1+}$ interface results in the formation of a twice as pronounced 2DEG in the KTO system by occupation of Ta $5d$ conduction-band states, predominantly d_{xy}, which is accompanied by ferroelectriclike displacements of the Ta ions in the substrate. We find that the broken inversion symmetry at the surface and the interface gives rise to an anisotropic Rashba spin splitting that exceeds the size of the superconducting gap. Surprisingly, it reaches values at the KTO interface that are comparable to Bi(111) surface states. The Ti and Ta d_{xy} orbitals in the substrate exhibit a fundamentally different response to SOC than the Ni $3d_{x^2-y^2}$ orbitals in the film, i.e., a predominantly cubic versus linear momentum dependence of the spin splitting. We observe a substantial reconstruction of the Ni $3d_{x^2-y^2}$-derived Fermi sheets at the surface due to the electrostatic doping, suggesting local modifications of the pairing mechanism. In conjunction with the surprisingly large Rashba effect, this may add a more exotic triplet component to the superconducting wave function. Finally, layerwise tracking of these

*benjamin.geisler@ufl.edu

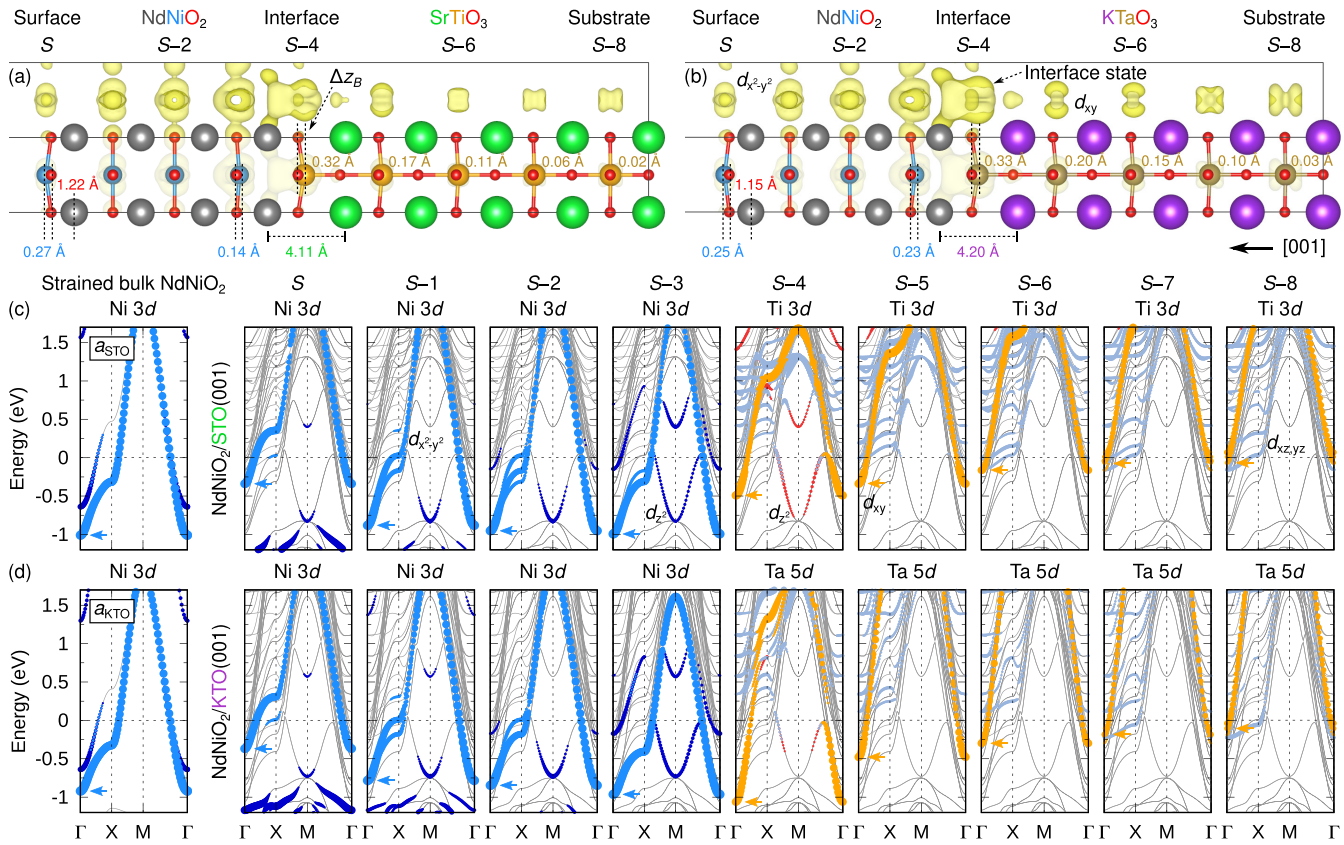

FIG. 1. Optimized geometry of (a) $(NdNiO_2)_4$/STO(001) [47] and (b) $(NdNiO_2)_4$/KTO(001), together with the electron density integrated between -0.75 eV and the Fermi energy. (c), (d) The corresponding layer-resolved band structures (here from DFT $+ U$ without SOC) show the polarity-driven emergence of an interfacial 2DEG in both substrates by occupation of Ti $3d$ and Ta $5d$ conduction-band states, respectively (orange arrows), as well as the electrostatic modulation of the Ni $3d$ states in the polar infinite-layer nickelate film (blue arrows). Light- and dark-blue bands depict Ni $d_{x^2-y^2}$ and d_{z^2} states; orange, gray-blue, and red bands depict Ti and Ta d_{xy}, $d_{xz,yz}$, and d_{z^2} states; and the thin gray lines represent the total band structure of the supercells. Results for strained bulk $NdNiO_2$ are provided as reference (left panels).

states throughout the nickelate film unveils a Lifshitz transition towards a cupratelike topology that coincides with a reorientation of their spin texture.

II. METHODOLOGY

We performed first-principles simulations in the framework of density functional theory (DFT [59]) as implemented in the VIENNA AB INITIO SIMULATION PACKAGE (VASP) [60,61], employing the PBE exchange-correlation functional [62] and a wave-function cutoff of 520 eV. Static correlation effects were considered within the DFT $+ U$ formalism [63,64] employing $U - J = 3$ eV at the Ni and Ti sites and $U - J = 1$ eV at the Ta sites, similar to previous work [26,47,51,65–72]. An assessment of the U dependence of the key results is compiled in the Supplemental Material (SM) [73]. Subsequent to a nonmagnetic self-consistent calculation [17,22,26,27,74], we shift to a spinor representation, account for spin-orbit interactions, and thus obtain an updated electronic structure. Additional results for a spin-polarized system can be found in the Appendix.

$(NdNiO_2)_4$/STO(001) and $(NdNiO_2)_4$/KTO(001) are modeled in explicit film geometry by using tetragonal supercells, fixing the in-plane lattice parameter to $a_{STO} = 3.905$ Å and $a_{KTO} = 3.988$ Å [55], respectively. The supercells are symmetric, consisting in total of 9.5 unit cells of substrate, $4 + 4$ unit cells of infinite-layer nickelate film, and about 20 Å of vacuum region.

The Brillouin zone was sampled employing a $16 \times 16 \times 1$ Monkhorst-Pack $\vec{k}$-point grid [75] in conjunction with a Gaussian smearing of 5 mRy. The ionic positions were accurately optimized in DFT $+ U$, reducing ionic forces below 1 mRy/a.u.

III. IONIC RELAXATIONS AND ELECTRONIC RECONSTRUCTION

Figures 1(a) and 1(b) show the optimized geometry of $(NdNiO_2)_4$/STO(001) [47] and $(NdNiO_2)_4$/KTO(001), respectively. The apical A-site distances are significantly enhanced at the interface $(S - 4)$ to $d_{\text{Nd-Sr}} = 4.11$ Å for STO and even $d_{\text{Nd-K}} = 4.20$ Å for KTO. This observation can be attributed to the electrostatic doping [47] and resembles the increased La-Sr distance at the n-type $LaNiO_3$/STO(001) interface (∼4.06 Å) [67,76,77]. Conversely, the distance between the surface NiO_2 layer (S) and the subsurface Nd layer is considerably contracted to 1.22 Å (STO) and 1.15 Å (KTO).

Both systems exhibit a prominent buckling of the NiO_2 layers at the surface (S) [Figs. 1(a) and 1(b)], the Ni ions being displaced outwards from the respective oxygen layer by $\Delta z_B = 0.27$ Å (STO) and 0.25 Å (KTO). At the interface ($S-3$), the Ni displacements point inwards and are more distinct, i.e., 0.14 Å (STO) and 0.23 Å (KTO). Furthermore, the Ti and Ta ions show a sizable inward ferroelectriclike displacement of $\Delta z_B \sim 0.3$ Å in layer $S-4$ that decays with increasing distance from the interface. Close comparison of the two systems reveals consistently larger displacements Δz_B in the KTO substrate (see also SM), even though bulk KTO is cubic and paraelectric down to at least 4.2 K [55,78,79]. In summary, these results point to a substantial difference between the two materials combinations.

The vertical ionic displacements are a sensitive response to the internal electric fields [47,51]. This becomes evident in Figs. 1(c) and 1(d), which compare the layer-resolved DFT + U electronic structure of the two systems. Similar to $NdNiO_2$/STO(001), the polar discontinuity at the $NdNiO_2$/KTO(001) interface drives the formation of a 2DEG due to the occupation of Ta 5d conduction-band states in the substrate, predominantly the planar d_{xy} orbitals, which are bent down by -1.06 eV at the Γ point in layer $S-4$. This electronic reconstruction and the orbital order present at the Ti and Ta sites are clearly visible in the electron density [Figs. 1(a) and 1(b)]. For comparison, the respective Ti 3d states bend down by -0.49 eV (-0.55 eV in Ref. [47]). The strongly enhanced Ta 5d occupation relative to Ti 3d can be traced back to the distinct 3+/1+ versus 3+/0 interface polarity. Similarly, the 2DEG near the pristine KTO(001) surface [52] is considerably less pronounced due to the absence of Nd^{3+} (see SM for a direct comparison). The band bending decays exponentially with increasing distance from the interface, paralleling the evolution of the ferroelectric-like displacements Δz_B. Hence, the potential well confining the 2DEG is considerably more asymmetric in $NdNiO_2$/KTO(001) than in $NdNiO_2$/STO(001). A concomitant electrostatic modulation of the Ni 3d states, specifically $d_{x^2-y^2}$, leads to an overall charge depletion (hole doping) in the polar films for both systems, particularly near the surface [Figs. 1(c) and 1(d)]. Simultaneously, the Ni d_{z^2} states located below -1 eV are fully occupied in all layers, similar to the bulk [26].

IV. ANISOTROPIC AND ORBITAL-SELECTIVE RASHBA EFFECT

We now explore the impact of SOC on the electronic structure at the surface of the nickelate film and in the 2DEG near the interface, where the electronic reconstruction is most pronounced. The polar discontinuities result in strong electric fields perpendicular to the basal conduction plane that are perceived as magnetic fields by a moving electron and thus couple to its spin. Specifically, this gives rise to the Rashba effect, which can be described by $H_R = \alpha_R(\vec{e}_z \times \vec{k}) \cdot \vec{\sigma}$, where $\vec{\sigma}$ is the Pauli vector and α_R is the Rashba coupling constant. The latter is a measure of the SOC strength and depends on the local electric fields [80]. It lifts the spin degeneracy of the bands and manifests as a linear splitting $\Delta(k) = 2\alpha_R k$ for a free-electron 2DEG model. First-principles simulations provide a more comprehensive perspective and allow us to explore the Rashba effect layer resolved, specifically the aspect of anisotropy, higher-order k^3 effects, and the distinct response of the different transition-metal d orbitals.

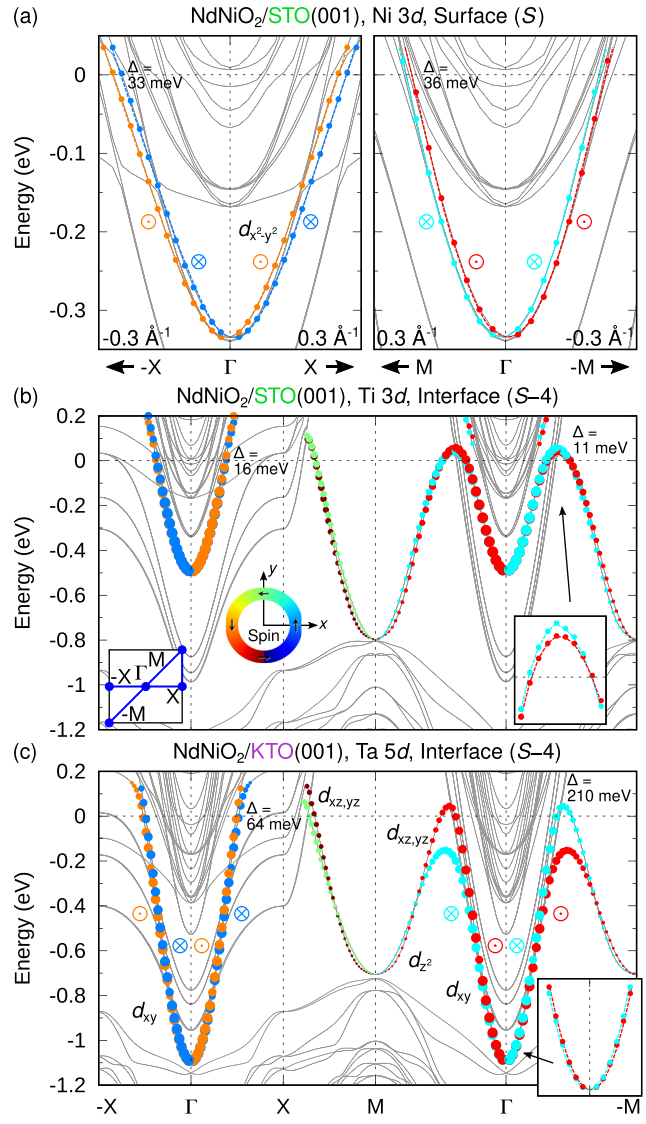

FIG. 2. DFT + U + SOC surface and interface electronic structure in $NdNiO_2$/STO(001) and $NdNiO_2$/KTO(001). The colored points represent the orbital projections, while the color encodes the spin direction in the xy plane. The splitting of bands with opposite spin is clearly visible (e.g., blue vs orange and cyan vs red points). (a) The Ni-3$d_{x^2-y^2}$-derived surface state (S), plotted exemplarily for $NdNiO_2$/STO(001) along two directions, displays the characteristic Rashba shape around the Γ point. (b), (c) The interface state ($S-4$) exhibits a similar effect, but with a massively boosted splitting in $NdNiO_2$/KTO(001). Intriguingly, the outer Ta 5d cone does not cross the Fermi energy along Γ-M, in sharp contrast to the inner cone. This behavior is fundamentally distinct from $NdNiO_2$/STO(001).

Figure 2(a) shows the Ni-3$d_{x^2-y^2}$-derived surface state in layer S, exemplarily for $NdNiO_2$/STO(001). We obtained similar results for $NdNiO_2$/KTO(001) and show below that a freestanding nickelate film provides equivalent results. The characteristic Rashba shape emerges around the Γ point in the

basal plane: The quasiparabolic band splits into two distinct cones of opposite spin (represented here by different colors). The spin splitting is anisotropic, reflecting the fourfold D_{4h} symmetry of the structure, and amounts to $\Delta = 33$ meV along Γ-X and 36 meV along Γ-M at the Fermi level. This corresponds to a wave vector of $\Delta k_{\parallel} \sim 0.02\,\text{Å}^{-1}$, which is surprisingly larger than $\Delta k_{\parallel} \sim 0.01\,\text{Å}^{-1}$ calculated for the polar KTO(001) surface [52], even though $NdNiO_2$ consists of much lighter elements and shows negligible impact of SOC in the bulk [81].

Next, we investigate the state in the first substrate layer [$S-4$; Figs. 2(b) and 2(c)]. Around the Γ point, it exhibits a quasiparabolic dispersion, indicative of the 2DEG, and predominantly d_{xy} orbital character. In $NdNiO_2$/STO(001) [Fig. 2(b)], the Rashba splitting at the Fermi level amounts to $\Delta = 16$ meV along Γ-X and 11 meV along Γ-M, which is smaller than the results obtained for the surface state. Interestingly, along Γ-M, the band bends down again after initially rising to ~0.05 eV, concomitantly changing its predominant orbital character from Ti d_{xy} to Ti $d_{xz,yz}$ and, finally, to Ni d_{z^2} at the M point. In contrast, the corresponding state in layer $S-5$ presents a consistently parabolic dispersion around the Γ point [cf. Figs. 1(c) and 1(d)].

For $NdNiO_2$/KTO(001) [Fig. 2(c)], the dispersion of the interface state is qualitatively similar to $NdNiO_2$/STO(001). However, the splitting along Γ-X is considerably enhanced to $\Delta = 64$ meV, which is four times as high as for the STO system. This demonstrates that shifting from $Z_{\text{Ti}} = 22$ to $Z_{\text{Ta}} = 73$ promotes the impact of SOC substantially. An additional contribution stems from the stronger asymmetry of the confining potential well in $NdNiO_2$/KTO(001), owing to the distinct interface polarity [Fig. 1(d)]. Intriguingly, we observe a spin splitting of $\Delta = 210$ meV along Γ-M, which is 19 times as high as for the STO system and reminiscent of Bi(111) surface states (~0.2 eV [82]; $Z_{\text{Bi}} = 83$). Even the shape of the spin-split bands bears a striking resemblance to Bi(111). A notable difference, however, is the suppressed contribution of the counterclockwise Ta 5d cone to the Fermi surface, in sharp contrast to the clockwise cone [Fig. 2(c)]. We verified this result, which is fundamentally distinct from $NdNiO_2$/STO(001), by performing fully self-consistent SOC calculations. Compellingly, the pristine KTO(001) surface lacks a comparable effect and exhibits a much smaller spin splitting [52].

Motivated by this observation, we analyze the momentum-resolved spin splitting $\Delta(k)$ of the states shown in Fig. 2 along two directions from the Γ point to roughly the Fermi wave vector k_{F} in Fig. 3. The data points show a clear nonlinearity, but can be accurately fitted to $\Delta(k) = 2\alpha_{\text{R}}k + 2\tilde{\alpha}_{\text{R}}k^3$ despite the broad k range. The three panels reveal the complexity of the Rashba effect in infinite-layer nickelate heterostructures. First, they underpin that $\Delta(k)$ is anisotropic and generally more pronounced along Γ-M. Surprisingly, $NdNiO_2$/STO(001) shows an inverted behavior in layer $S-4$, with a stronger splitting along Γ-X [Fig. 3(b)]. Second, the $d_{x^2-y^2}$-derived states in the nickelate film exhibit a fundamentally distinct response to SOC than the d_{xy}-derived states in the substrate, albeit both orbitals are planar. At the surface, the linear term is very strong ($\alpha_{\text{R}} \sim 125$ meV Å, Table I). Simultaneously, $\tilde{\alpha}_{\text{R}} \sim -1.1$ eV Å^3 is highly negative due

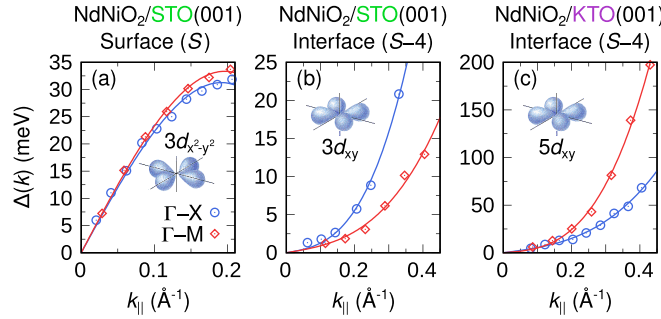

FIG. 3. Momentum-resolved spin splitting $\Delta(k)$ around the Γ point for selected layers of (a), (b) $NdNiO_2$/STO(001) and (c) $NdNiO_2$/KTO(001) from DFT + U + SOC (symbols; cf. Fig. 2). The lines represent fits to $\Delta(k) = 2\alpha_{\text{R}}k + 2\tilde{\alpha}_{\text{R}}k^3$ (Table I). The qualitative differences between the three panels reflect the orbital selectivity of the anisotropic Rashba effect at the surface versus interface, as well as the role of lighter versus heavier substrate elements.

to a profound nonlinearity for $k > 0.1\,\text{Å}^{-1}$ [Fig. 3(a)]. In sharp contrast, the substrate layers feature a dominant k^3 term with positive $\tilde{\alpha}_{\text{R}}$ [Figs. 3(b) and 3(c), Table I]. The linear term is at least one order of magnitude smaller than at the surface and decays with increasing distance to the interface. Despite this orbital selectivity, α_{R} is not fully quenched by symmetry, as suggested for the KTO(001) surface [52]. Finally, the role of heavier versus lighter substrate elements manifests in massively enhanced Rashba constants α_{R} and $\tilde{\alpha}_{\text{R}}$ near the $NdNiO_2$/KTO(001) interface (Table I), in line with the boosted splittings Δ discussed above. For instance, α_{R} differs by one order of magnitude. Interestingly, the massive splitting of 210 meV observed along Γ-M in the KTO system is perfectly captured by the fit [Fig. 3(c)] and thus emerges as strong nonlinear k^3 response ($\tilde{\alpha}_{\text{R}} \sim 1.2$ eV Å^3) of the d_{xy} orbitals.

At the $NdNiO_2$/KTO(001) interface, α_{R} reaches ~24 meV Å (Table I), which compares favorably to ~20 meV Å for $LaAlO_3$/STO(001) determined from magnetotransport measurements [13]. Moreover, all Rashba splittings observed here exceed ~4 meV reported for $LaAlO_3$/STO(001) [13]. In particular, they are one to

TABLE I. Rashba constants α_{R} (meV Å) and $\tilde{\alpha}_{\text{R}}$ (meV Å^3) obtained by fitting the DFT + U + SOC data for the surface and two substrate layers near the interface (cf. Fig. 3). Additionally, the corresponding spin splitting energy Δ (meV) at the Fermi level is provided.

System		—— Γ-X ——			—— Γ-M ——		
Layer	Orbital	Δ	α_{R}	$\tilde{\alpha}_{\text{R}}$	Δ	α_{R}	$\tilde{\alpha}_{\text{R}}$
$NdNiO_2$/STO(001)							
S	Ni $3d_{x^2-y^2}$	33	123	−1116	36	128	−1107
$S-4$	Ti $3d_{xy}$	16	3.9	251	11	3.8	79
$S-5$	Ti $3d_{xy}$	8	2.4	278	10	1.5	405
$NdNiO_2$/KTO(001)							
S	Ni $3d_{x^2-y^2}$	32	119	−1092	35	123	−1052
$S-4$	Ta $5d_{xy}$	64	24	355	210	14	1185
$S-5$	Ta $5d_{xy}$	15	14	409	36	11	972

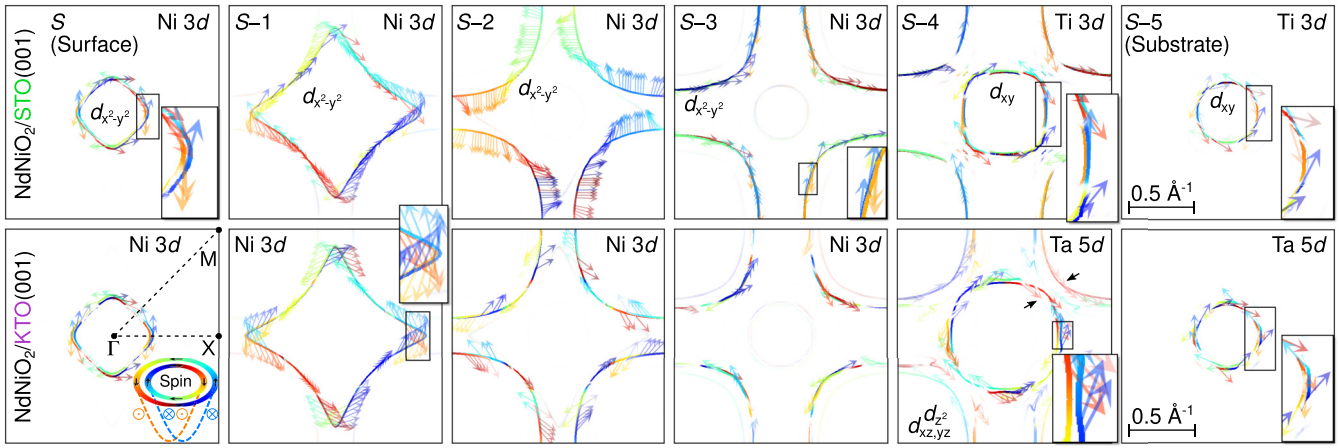

FIG. 4. Layer-resolved Fermi surface of $(NdNiO_2)_4/STO(001)$ (top) and $(NdNiO_2)_4/KTO(001)$ (bottom). The line intensity represents the respective d orbital character, whereas the color and arrows indicate the basal spin direction (cf. Fig. 2). The reconstructed Ni $3d_{x^2-y^2}$-derived Fermi sheet at the surface undergoes a Lifshitz transition towards a cupratelike topology deeper in the film, accompanied by a realignment of the spin texture. Spin-orbit interactions generally split each contribution into two distinct sheets of opposite spin. An exception is the single-band zones along Γ-M resulting from the suppression of the counter-clockwise Ta 5d cone at the interface [black arrows; cf. Fig. 2(c)].

two orders of magnitude larger than the superconducting gap, which amounts to 2–4 meV in 12–25% Sr-doped $NdNiO_2$ films on STO(001) according to scanning tunneling spectroscopy [30]. Therefore, spin-orbit effects turn out to be a key ingredient in describing the interactions between the superconducting infinite-layer nickelate film and the 2DEG in the substrate.

V. LIFSHITZ TRANSITION AND SPIN TEXTURE

Finally, we investigate the Fermi surface and the corresponding spin texture of $NdNiO_2/STO(001)$ and $NdNiO_2/KTO(001)$. Figure 4 disentangles the d-orbital contributions from subsequent BO_2 layers, similar to the layer-resolved band structure in Fig. 1. Owing to the electrostatic doping, each layer exhibits a distinct Fermi sheet of unique shape. Spin-orbit interactions generally split each contribution into two sheets of opposite spin, e.g., clockwise versus counter-clockwise spin rotation, which is indicative of the underlying Rashba spin-orbit physics [83].

At the surface of the nickelate film (S), we observe a significantly reconstructed Ni-$3d_{x^2-y^2}$-derived sheet of almost circular shape centered around the Γ point. The reconstruction can be attributed to the electrostatic doping and suggests substantial modifications of the local pairing mechanism [84]. Moreover, the unexpectedly large Rashba effect can drive the emergence of a finite triplet pairing component [85]; further exploration in the context of magnetic interactions [31,40,81,86,87] will be of interest. Finally, these insights may be key in the interpretation of scanning tunneling spectroscopy results [30]. This is of particular relevance since, based on these measurements, it has recently been argued that the superconductivity in infinite-layer nickelates is conventional [88]. On the other hand, the considerable Ni-O buckling at the surface (cf. Fig. 1) rather evokes parallels to Fe-based superconductors [89].

From layer $S-1$ to layer $S-2$, a topological transition of the Fermi sheets to a cupratelike shape occurs. This Lifshitz transition [90,91] is accompanied by a reorientation of the spins, which ultimately form a closed loop around the M point ($S-3$). The Fermi sheets are degenerate for layer $S-2$, whereas layers $S-1$ and $S-3$ present a clear Rashba splitting.

At the interface ($S-4$), the d_{xy}-derived 2DEG sheets centered around the Γ point are combined with $d_{xz,yz}$ and d_{z^2} contributions centered around the M point. The enhanced splitting in $NdNiO_2/KTO(001)$ is clearly visible (cf. Table I). Interestingly, single-band zones emerge along Γ-M due to the suppression of the counter-clockwise Ta 5d cone (black arrows in Fig. 4). In turn, weak $d_{xz,yz}$ signatures appear around the X point that are absent in the STO system. The overall shape of the Fermi sheet and its spin texture is reminiscent of the oxygen-deficient (i.e., n-type) STO(001) surface [92]. Finally, layer $S-5$ presents a quasicircular Rashba-split 2DEG sheet of exclusive d_{xy} character centered around the Γ point.

VI. SUMMARY

We investigated the impact of spin-orbit interactions in $NdNiO_2/SrTiO_3(001)$ and $NdNiO_2/KTaO_3(001)$ in explicit film geometry. First-principles simulations unraveled that the distinct polarity mismatch at the $Nd^{3+}/(TiO_2)^0$ versus $Nd^{3+}/(TaO_2)^{1+}$ interface results in the emergence of a 2DEG in $NdNiO_2/KTaO_3(001)$ that is twice as pronounced as in $NdNiO_2/SrTiO_3(001)$ and involves the occupation of Ta 5d conduction-band states, predominantly d_{xy}. Ferroelectriclike displacements of the Ta ions in the substrate act as a fingerprint of this electronic reconstruction. We identified an anisotropic Rashba spin splitting of the states at the surface and the interface that exceeds the size of the superconducting gap, which establishes spin-orbit effects as crucial ingredient in describing the superconductor–2DEG coupling. At the $KTaO_3$ interface, the splitting reaches 210 meV, which is reminiscent of Bi(111) surface states. The predominantly cubic momentum dependence of the spin splitting exhibited by the substrate Ti and Ta d_{xy} states contrasts with a surprisingly

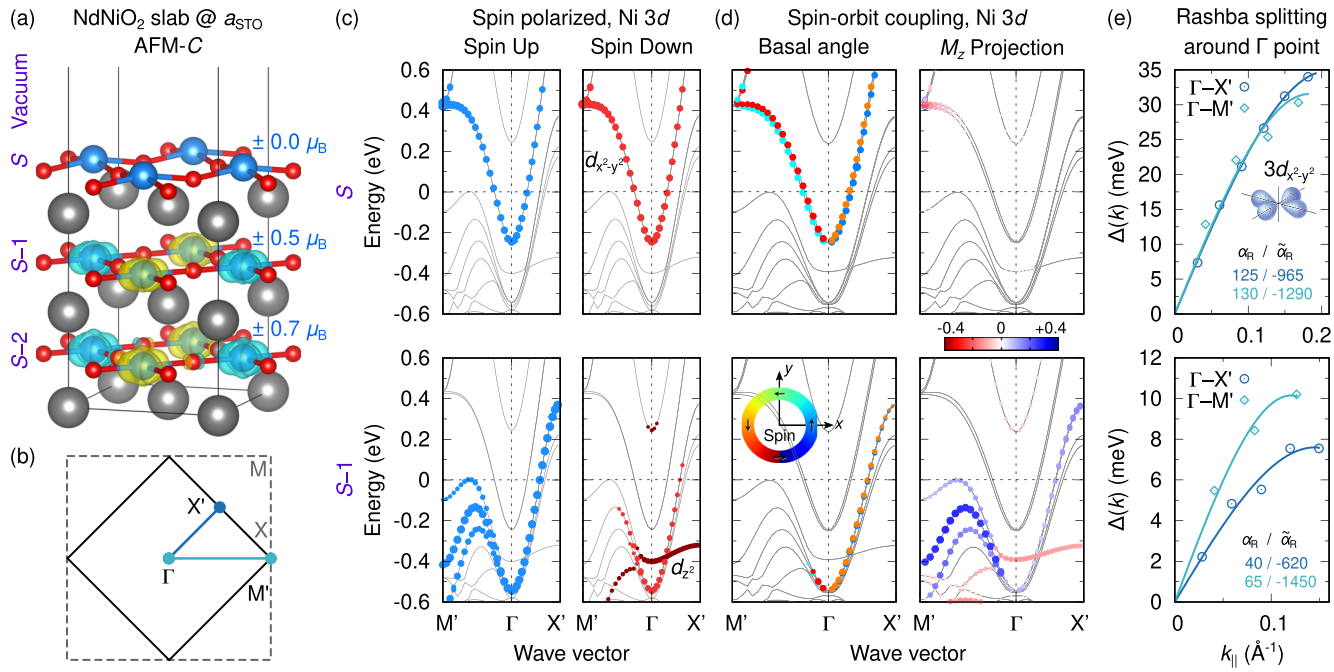

FIG. 5. (a) Optimized geometry of a strained $(NdNiO_2)_{5.5}$ slab in the C-type AFM state. The isosurfaces represent the spin density (yellow/blue corresponding to positive/negative). (b) Relations between the 1×1 (nonmagnetic, grey) and $\sqrt{2} \times \sqrt{2}$ (AFM, black) Brillouin zones and the respective labels of the high-symmetry points. (c) Spin-resolved DFT $+ U$ band structure, projected on the Ni $3d$ states in layers S (top tow) and $S - 1$ (bottom row) at a site with positive magnetic moment. (d) DFT $+ U +$ SOC band structure. The basal spin direction is color encoded as in Fig. 2. Additionally, the expectation value M_z in apical direction is provided (in arbitrary units). (e) Momentum-resolved spin splitting $\Delta(k)$ around the Γ point in layers S (top tow) and $S - 1$ (bottom row), similar to the analysis shown in Fig. 3.

strong linear component presented by the Ni $3d_{x^2-y^2}$ orbitals in the film, which exemplifies the orbital selectivity of the Rashba effect and may lead to a finite triplet component in the superconducting wave function. Finally, we observed a reconstructed, quasicircular Ni $3d_{x^2-y^2}$-derived Fermi sheet at the surface, owing to the electrostatic doping, which undergoes a Lifshitz transition towards a cupratelike topology and a concomitant realignment of its spin texture deeper in the film. These results suggest surface and interface polarity as promising control parameters to tune spin-orbit physics and the pairing mechanism in superconducting infinite-layer nickelate heterostructures.

ACKNOWLEDGMENTS

This work was funded by the National Science Foundation via Grant No. NSF-DMR-2118718, which is gratefully acknowledged. The author thanks A. Sahinovic, Dr. O. Köksal, Dr. A. Kreisel, Professor R. Pentcheva, Professor R. G. Hennig, and Professor P. J. Hirschfeld for their support, helpful comments, and numerous discussions.

APPENDIX: RASHBA EFFECT IN AN ANTIFERROMAGNETICALLY ORDERED $NdNiO_2$ SLAB

The results discussed so far are based on non-spin-polarized charge densities of oxide heterostructures. To obtain a first impression of the impact of a (possible) finite spin polarization in the nickelate film, here we discuss results for a (strained) $NdNiO_2$ surface slab in the C-type antiferromagnetic (AFM) state [81,93]. The symmetric $(NdNiO_2)_{5.5}$ slab comprises six NiO_2 layers in total and includes a vacuum region [Fig. 5(a)]. To account for the checkerboard spin pattern, the lateral cell size has been doubled to $\sqrt{2}\,a_{STO} \times \sqrt{2}\,a_{STO}$.

Intriguingly, the Ni magnetic moments at the (001) surface collapse [Fig. 5(a), S], rendering a situation close to the nonmagnetic state explored above. This magnetic reconstruction agrees with earlier theoretical findings for $NdNiO_2$ films where a G-type AFM configuration was assumed [50]. We therefore speculate that a similar phenomenon would also occur in a paramagnetic state. The surface band is of Ni $3d_{x^2-y^2}$ character [Fig. 5(c)]. It crosses the Fermi energy along $\Gamma - X'$ and $\Gamma - M'$, which implies a significantly reconstructed Fermi surface topology, as reported above (Fig. 4). When spin-orbit interactions are included, the surface band presents the characteristic Rashba splitting [Fig. 5(d)]. Simultaneously, the M_z projections vanish, i.e., the (pseudo)spins align in the basal plane. We find that the linear Rashba term is very strong ($\alpha_R \sim 125$–130 meV Å), and that the Rashba splitting $\Delta(k)$ reaches 30–35 meV [Fig. 5(e)]. These values agree surprisingly closely with the observations we discussed above (Fig. 3, Table I), which demonstrates that our results for the $NdNiO_2$/STO(001) and $NdNiO_2$/KTO(001) surfaces are also applicable for freestanding $NdNiO_2$ slabs.

In layer $S - 1$, we identify finite magnetic moments of $\pm 0.5 \mu_B$ at the Ni sites [Fig. 5(a)]. The respective bands of Ni $3d_{x^2-y^2}$ character cross the Fermi energy exclusively along $\Gamma - X'$ [Fig. 5(c)], in sharp contrast to the surface layer. Around -0.4 eV, Ni $3d_{z^2}$ contributions can be observed in the spin-down channel. Spin-orbit coupling induces finite

basal spin components (M_x, M_y) solely for the Ni-$3d_{x^2-y^2}$-derived band along $\Gamma - X'$, accompanied by monotonically increasing M_z contributions [Fig. 5(d)]. Along $\Gamma - M'$, the M_z component is dominant, and finite basal components can only be observed close to the Γ point. The Rashba splitting $\Delta(k)$ arises exclusively in conjunction with these basal components and reaches 8–10 meV in layer $S-1$. Again, the linear term is sizable ($\alpha_R \sim 40$–65 meV Å), particularly along $\Gamma - M'$ [Fig. 5(e)], albeit less pronounced than at the surface (S) due to the smaller electrostatic potential gradient. This reduction is consistent with the observations reported above for layer $S-1$ in $NdNiO_2$/STO(001) and $NdNiO_2$/KTO(001) (Fig. 4).

[1] Y. A. Bychkov and E. I. Rashba, Oscillatory effects and the magnetic susceptibility of carriers in inversion layers, J. Phys. C **17**, 6039 (1984).

[2] I. Žutić, J. Fabian, and S. Das Sarma, Spintronics: Fundamentals and applications, Rev. Mod. Phys. **76**, 323 (2004).

[3] R. M. Lutchyn, J. D. Sau, and S. Das Sarma, Majorana fermions and a topological phase transition in semiconductor-superconductor heterostructures, Phys. Rev. Lett. **105**, 077001 (2010).

[4] Y. Oreg, G. Refael, and F. von Oppen, Helical liquids and Majorana bound states in quantum wires, Phys. Rev. Lett. **105**, 177002 (2010).

[5] R. M. Lutchyn, E. P. A. M. Bakkers, L. P. Kouwenhoven, P. Krogstrup, C. M. Marcus, and Y. Oreg, Majorana zero modes in superconductor–semiconductor heterostructures, Nat. Rev. Mater. **3**, 52 (2018).

[6] M. Lorenz, M. S. R. Rao, T. Venkatesan, E. Fortunato, P. Barquinha, R. Branquinho, D. Salgueiro, R. Martins, E. Carlos, A. Liu, F. K. Shan, M. Grundmann, H. Boschker, J. Mukherjee, M. Priyadarshini, N. DasGupta, D. J. Rogers, F. H. Teherani, E. V. Sandana, P. Bove *et al.*, The 2016 oxide electronic materials and oxide interfaces roadmap, J. Phys. D: Appl. Phys. **49**, 433001 (2016).

[7] A. Ohtomo and H. Y. Hwang, A high-mobility electron gas at the $LaAlO_3/SrTiO_3$ heterointerface, Nature (London) **427**, 423 (2004).

[8] N. Nakagawa, H. Y. Hwang, and D. A. Muller, Why some interfaces cannot be sharp, Nat. Mater. **5**, 204 (2006).

[9] S. Thiel, G. Hammerl, A. Schmehl, C. W. Schneider, and J. Mannhart, Tunable quasi-two-dimensional electron gases in oxide heterostructures, Science **313**, 1942 (2006).

[10] R. Pentcheva and W. E. Pickett, Avoiding the polarization catastrophe in $LaAlO_3$ overlayers on $SrTiO_3$(001) through polar distortion, Phys. Rev. Lett. **102**, 107602 (2009).

[11] C. Bell, S. Harashima, Y. Kozuka, M. Kim, B. G. Kim, Y. Hikita, and H. Y. Hwang, Dominant mobility modulation by the electric field effect at the $LaAlO_3/SrTiO_3$ interface, Phys. Rev. Lett. **103**, 226802 (2009).

[12] N. Reyren, S. Thiel, A. D. Caviglia, L. F. Kourkoutis, G. Hammerl, C. Richter, C. W. Schneider, T. Kopp, A.-S. Rüetschi, D. Jaccard, M. Gabay, D. A. Muller, J.-M. Triscone, and J. Mannhart, Superconducting interfaces between insulating oxides, Science **317**, 1196 (2007).

[13] A. D. Caviglia, M. Gabay, S. Gariglio, N. Reyren, C. Cancellieri, and J.-M. Triscone, Tunable Rashba spin-orbit interaction at oxide interfaces, Phys. Rev. Lett. **104**, 126803 (2010).

[14] M. Ben Shalom, M. Sachs, D. Rakhmilevitch, A. Palevski, and Y. Dagan, Tuning spin-orbit coupling and superconductivity at the $SrTiO_3/LaAlO_3$ interface: A magnetotransport study, Phys. Rev. Lett. **104**, 126802 (2010).

[15] D. A. Dikin, M. Mehta, C. W. Bark, C. M. Folkman, C. B. Eom, and V. Chandrasekhar, Coexistence of superconductivity and ferromagnetism in two dimensions, Phys. Rev. Lett. **107**, 056802 (2011).

[16] K. Michaeli, A. C. Potter, and P. A. Lee, Superconducting and ferromagnetic phases in $SrTiO_3/LaAlO_3$ oxide interface structures: Possibility of finite momentum pairing, Phys. Rev. Lett. **108**, 117003 (2012).

[17] D. Li, K. Lee, B. Y. Wang, M. Osada, S. Crossley, H. R. Lee, Y. Cui, Y. Hikita, and H. Y. Hwang, Superconductivity in an infinite-layer nickelate, Nature (London) **572**, 624 (2019).

[18] D. Li, B. Y. Wang, K. Lee, S. P. Harvey, M. Osada, B. H. Goodge, L. F. Kourkoutis, and H. Y. Hwang, Superconducting dome in $Nd_{1-x}Sr_xNiO_2$ infinite layer films, Phys. Rev. Lett. **125**, 027001 (2020).

[19] M. Osada, B. Y. Wang, B. H. Goodge, K. Lee, H. Yoon, K. Sakuma, D. Li, M. Miura, L. F. Kourkoutis, and H. Y. Hwang, A superconducting praseodymium nickelate with infinite layer structure, Nano Lett. **20**, 5735 (2020).

[20] S. Zeng, C. S. Tang, X. Yin, C. Li, M. Li, Z. Huang, J. Hu, W. Liu, G. J. Omar, H. Jani, Z. S. Lim, K. Han, D. Wan, P. Yang, S. J. Pennycook, A. T. S. Wee, and A. Ariando, Phase diagram and superconducting dome of infinite-layer $Nd_{1-x}Sr_xNiO_2$ thin films, Phys. Rev. Lett. **125**, 147003 (2020).

[21] M. Osada, B. Y. Wang, B. H. Goodge, S. P. Harvey, K. Lee, D. Li, L. F. Kourkoutis, and H. Y. Hwang, Nickelate superconductivity without rare-earth magnetism: (La, Sr)NiO_2, Adv. Mater. **33**, 2104083 (2021).

[22] Y. Nomura, M. Hirayama, T. Tadano, Y. Yoshimoto, K. Nakamura, and R. Arita, Formation of a two-dimensional single-component correlated electron system and band engineering in the nickelate superconductor $NdNiO_2$, Phys. Rev. B **100**, 205138 (2019).

[23] P. Jiang, L. Si, Z. Liao, and Z. Zhong, Electronic structure of rare-earth infinite-layer $RNiO_2$ (R = La, Nd), Phys. Rev. B **100**, 201106(R) (2019).

[24] H. Sakakibara, H. Usui, K. Suzuki, T. Kotani, H. Aoki, and K. Kuroki, Model construction and a possibility of cupratelike pairing in a new d^9 nickelate superconductor (Nd,Sr)NiO_2, Phys. Rev. Lett. **125**, 077003 (2020).

[25] M. Jiang, M. Berciu, and G. A. Sawatzky, Critical nature of the Ni spin state in doped $NdNiO_2$, Phys. Rev. Lett. **124**, 207004 (2020).

[26] A. S. Botana and M. R. Norman, Similarities and differences between $LaNiO_2$ and $CaCuO_2$ and implications for superconductivity, Phys. Rev. X **10**, 011024 (2020).

[27] F. Lechermann, Late transition metal oxides with infinite-layer structure: Nickelates versus cuprates, Phys. Rev. B **101**, 081110(R) (2020).

[28] L. Si, W. Xiao, J. Kaufmann, J. M. Tomczak, Y. Lu, Z. Zhong, and K. Held, Topotactic hydrogen in nickelate

superconductors and akin infinite-layer oxides ABO_2, Phys. Rev. Lett. **124**, 166402 (2020).

[29] X. Wu, D. Di Sante, T. Schwemmer, W. Hanke, H. Y. Hwang, S. Raghu, and R. Thomale, Robust $d_{x^2-y^2}$-wave superconductivity of infinite-layer nickelates, Phys. Rev. B **101**, 060504(R) (2020).

[30] Q. Gu, Y. Li, S. Wan, H. Li, W. Guo, H. Yang, Q. Li, X. Zhu, X. Pan, Y. Nie, and H.-H. Wen, Single particle tunneling spectrum of superconducting $Nd_{1-x}Sr_xNiO_2$ thin films, Nat. Commun. **11**, 6027 (2020).

[31] H. Lu, M. Rossi, A. Nag, M. Osada, D. F. Li, K. Lee, B. Y. Wang, M. Garcia-Fernandez, S. Agrestini, Z. X. Shen, E. M. Been, B. Moritz, T. P. Devereaux, J. Zaanen, H. Y. Hwang, K.-J. Zhou, and W. S. Lee, Magnetic excitations in infinite-layer nickelates, Science **373**, 213 (2021).

[32] R. A. Ortiz, H. Menke, F. Misják, D. T. Mantadakis, K. Fürsich, E. Schierle, G. Logvenov, U. Kaiser, B. Keimer, P. Hansmann, and E. Benckiser, Superlattice approach to doping infinite-layer nickelates, Phys. Rev. B **104**, 165137 (2021).

[33] F. Lechermann, Doping-dependent character and possible magnetic ordering of $NdNiO_2$, Phys. Rev. Mater. **5**, 044803 (2021).

[34] A. Sahinovic and B. Geisler, Active learning and element-embedding approach in neural networks for infinite-layer versus perovskite oxides, Phys. Rev. Res. **3**, L042022 (2021).

[35] B. Y. Wang, D. Li, B. H. Goodge, K. Lee, M. Osada, S. P. Harvey, L. F. Kourkoutis, M. R. Beasley, and H. Y. Hwang, Isotropic Pauli-limited superconductivity in the infinite-layer nickelate $Nd_{0.775}Sr_{0.225}NiO_2$, Nat. Phys. **17**, 473 (2021).

[36] C.-J. Kang and G. Kotliar, Optical properties of the infinite-layer $La_{1-x}Sr_xNiO_2$ and hidden Hund's physics, Phys. Rev. Lett. **126**, 127401 (2021).

[37] S. W. Zeng, X. M. Yin, C. J. Li, L. E. Chow, C. S. Tang, K. Han, Z. Huang, Y. Cao, D. Y. Wan, Z. T. Zhang, Z. S. Lim, C. Z. Diao, P. Yang, A. T. S. Wee, S. J. Pennycook, and A. Ariando, Observation of perfect diamagnetism and interfacial effect on the electronic structures in infinite layer $Nd_{0.8}Sr_{0.2}NiO_2$ superconductors, Nat. Commun. **13**, 743 (2022).

[38] A. Kreisel, B. M. Andersen, A. T. Rømer, I. M. Eremin, and F. Lechermann, Superconducting instabilities in strongly correlated infinite-layer nickelates, Phys. Rev. Lett. **129**, 077002 (2022).

[39] M. Rossi, M. Osada, J. Choi, S. Agrestini, D. Jost, Y. Lee, H. Lu, B. Y. Wang, K. Lee, A. Nag, Y.-D. Chuang, C.-T. Kuo, S.-J. Lee, B. Moritz, T. P. Devereaux, Z.-X. Shen, J.-S. Lee, K.-J. Zhou, H. Y. Hwang, and W.-S. Lee, A broken translational symmetry state in an infinite-layer nickelate, Nat. Phys. **18**, 869 (2022).

[40] J. Fowlie, M. Hadjimichael, M. M. Martins, D. Li, M. Osada, B. Y. Wang, K. Lee, Y. Lee, Z. Salman, T. Prokscha, J.-M. Triscone, H. Y. Hwang, and A. Suter, Intrinsic magnetism in superconducting infinite-layer nickelates, Nat. Phys. **18**, 1043 (2022).

[41] A. Sahinovic and B. Geisler, Quantifying transfer learning synergies in infinite-layer and perovskite nitrides, oxides, and fluorides, J. Phys.: Condens. Matter **34**, 214003 (2022).

[42] N. N. Wang, M. W. Yang, Z. Yang, K. Y. Chen, H. Zhang, Q. H. Zhang, Z. H. Zhu, Y. Uwatoko, L. Gu, X. L. Dong, J. P. Sun, K. J. Jin, and J.-G. Cheng, Pressure-induced monotonic enhancement of T_c to over 30 k in superconducting $Pr_{0.82}Sr_{0.18}NiO_2$ thin films, Nat. Commun. **13**, 4367 (2022).

[43] G. A. Pan, D. Ferenc Segedin, H. LaBollita, Q. Song, E. M. Nica, B. H. Goodge, A. T. Pierce, S. Doyle, S. Novakov, D. Córdova Carrizales, A. T. N'Diaye, P. Shafer, H. Paik, J. T. Heron, J. A. Mason, A. Yacoby, L. F. Kourkoutis, O. Erten, C. M. Brooks, A. S. Botana *et al.*, Superconductivity in a quintuple-layer square-planar nickelate, Nat. Mater. **21**, 160 (2022).

[44] B. H. Goodge, B. Geisler, K. Lee, M. Osada, B. Y. Wang, D. Li, H. Y. Hwang, R. Pentcheva, and L. F. Kourkoutis, Resolving the polar interface of infinite-layer nickelate thin films, Nat. Mater. **22**, 466 (2023).

[45] Q. Li, C. He, J. Si, X. Zhu, Y. Zhang, and H.-H. Wen, Absence of superconductivity in bulk $Nd_{1-x}Sr_xNiO_2$, Commun. Mater. **1**, 16 (2020).

[46] B.-X. Wang, H. Zheng, E. Krivyakina, O. Chmaissem, P. P. Lopes, J. W. Lynn, L. C. Gallington, Y. Ren, S. Rosenkranz, J. F. Mitchell, and D. Phelan, Synthesis and characterization of bulk $Nd_{1-x}Sr_xNiO_2$ and $Nd_{1-x}Sr_xNiO_3$, Phys. Rev. Mater. **4**, 084409 (2020).

[47] B. Geisler and R. Pentcheva, Fundamental difference in the electronic reconstruction of infinite-layer versus perovskite neodymium nickelate films on $SrTiO_3$(001), Phys. Rev. B **102**, 020502(R) (2020).

[48] F. Bernardini and A. Cano, Stability and electronic properties of $LaNiO_2/SrTiO_3$ heterostructures, Journal of Physics: Materials **3**, 03LT01 (2020).

[49] R. He, P. Jiang, Y. Lu, Y. Song, M. Chen, M. Jin, L. Shui, and Z. Zhong, Polarity-induced electronic and atomic reconstruction at $NdNiO_2/SrTiO_3$ interfaces, Phys. Rev. B **102**, 035118 (2020).

[50] Y. Zhang, L.-F. Lin, W. Hu, A. Moreo, S. Dong, and E. Dagotto, Similarities and differences between nickelate and cuprate films grown on a $SrTiO_3$ substrate, Phys. Rev. B **102**, 195117 (2020).

[51] B. Geisler and R. Pentcheva, Correlated interface electron gas in infinite-layer nickelate versus cuprate films on $SrTiO_3$(001), Phys. Rev. Res. **3**, 013261 (2021).

[52] P. D. C. King, R. H. He, T. Eknapakul, P. Buaphet, S.-K. Mo, Y. Kaneko, S. Harashima, Y. Hikita, M. S. Bahramy, C. Bell, Z. Hussain, Y. Tokura, Z.-X. Shen, H. Y. Hwang, F. Baumberger, and W. Meevasana, Subband structure of a two-dimensional electron gas formed at the polar surface of the strong spin-orbit perovskite $KTaO_3$, Phys. Rev. Lett. **108**, 117602 (2012).

[53] C. Liu, X. Yan, D. Jin, Y. Ma, H.-W. Hsiao, Y. Lin, T. M. Bretz-Sullivan, X. Zhou, J. Pearson, B. Fisher, J. S. Jiang, W. Han, J.-M. Zuo, J. Wen, D. D. Fong, J. Sun, H. Zhou, and A. Bhattacharya, Two-dimensional superconductivity and anisotropic transport at $KTaO_3$ (111) interfaces, Science **371**, 716 (2021).

[54] Z. Chen, Z. Liu, Y. Sun, X. Chen, Y. Liu, H. Zhang, H. Li, M. Zhang, S. Hong, T. Ren, C. Zhang, H. Tian, Y. Zhou, J. Sun, and Y. Xie, Two-dimensional superconductivity at the $LaAlO_3/KTaO_3$(110) heterointerface, Phys. Rev. Lett. **126**, 026802 (2021).

[55] A. Gupta, H. Silotia, A. Kumari, M. Dumen, S. Goyal, R. Tomar, N. Wadehra, P. Ayyub, and S. Chakraverty, $KTaO_3$—the new kid on the spintronics block, Adv. Mater. **34**, 2106481 (2022).

[56] K. Zou, S. Ismail-Beigi, K. Kisslinger, X. Shen, D. Su, F. J. Walker, and C. H. Ahn, $LaTiO_3/KTaO_3$ interfaces: A new

two-dimensional electron gas system, APL Mater. **3**, 036104 (2015).

[57] H. Zhang, X. Yan, X. Zhang, S. Wang, C. Xiong, H. Zhang, S. Qi, J. Zhang, F. Han, N. Wu, B. Liu, Y. Chen, B. Shen, and J. Sun, Unusual electric and optical tuning of $KTaO_3$-based two-dimensional electron gases with 5*d* orbitals, ACS Nano **13**, 609 (2019).

[58] N. Wadehra, R. Tomar, R. M. Varma, R. K. Gopal, Y. Singh, S. Dattagupta, and S. Chakraverty, Planar hall effect and anisotropic magnetoresistance in polar-polar interface of $LaVO_3$-$KTaO_3$ with strong spin-orbit coupling, Nat. Commun. **11**, 874 (2020).

[59] W. Kohn and L. J. Sham, Self-consistent equations including exchange and correlation effects, Phys. Rev. **140**, A1133 (1965).

[60] G. Kresse and D. Joubert, From ultrasoft pseudopotentials to the projector augmented-wave method, Phys. Rev. B **59**, 1758 (1999).

[61] P. E. Blöchl, Projector augmented-wave method, Phys. Rev. B **50**, 17953 (1994).

[62] J. P. Perdew, K. Burke, and M. Ernzerhof, Generalized gradient approximation made simple, Phys. Rev. Lett. **77**, 3865 (1996).

[63] A. I. Liechtenstein, V. I. Anisimov, and J. Zaanen, Density-functional theory and strong interactions: Orbital ordering in Mott-Hubbard insulators, Phys. Rev. B **52**, R5467 (1995).

[64] S. L. Dudarev, G. A. Botton, S. Y. Savrasov, C. J. Humphreys, and A. P. Sutton, Electron-energy-loss spectra and the structural stability of nickel oxide: An LSDA + U study, Phys. Rev. B **57**, 1505 (1998).

[65] J. Liu, M. Kargarian, M. Kareev, B. Gray, P. J. Ryan, A. Cruz, N. Tahir, Y.-D. Chuang, J. Guo, J. M. Rondinelli, J. W. Freeland, G. A. Fiete, and J. Chakhalian, Heterointerface engineered electronic and magnetic phases of $NdNiO_3$ thin films, Nat. Commun. **4**, 2714 (2013).

[66] H. Guo, S. Gangopadhyay, O. Köksal, R. Pentcheva, and W. E. Pickett, Wide gap Chern Mott insulating phases achieved by design, npj Quantum Mater. **2**, 4 (2017).

[67] B. Geisler, A. Blanca-Romero, and R. Pentcheva, Design of *n*- and *p*-type oxide thermoelectrics in $LaNiO_3/SrTiO_3$(001) superlattices exploiting interface polarity, Phys. Rev. B **95**, 125301 (2017).

[68] F. Wrobel, B. Geisler, Y. Wang, G. Christiani, G. Logvenov, M. Bluschke, E. Schierle, P. A. van Aken, B. Keimer, R. Pentcheva, and E. Benckiser, Digital modulation of the nickel valence state in a cuprate-nickelate heterostructure, Phys. Rev. Mater. **2**, 035001 (2018).

[69] B. Geisler and R. Pentcheva, Confinement- and strain-induced enhancement of thermoelectric properties in $LaNiO_3$/$LaAlO_3$(001) superlattices, Phys. Rev. Mater. **2**, 055403 (2018).

[70] B. Geisler and R. Pentcheva, Inducing *n*- and *p*-type thermoelectricity in oxide superlattices by strain tuning of orbital-selective transport resonances, Phys. Rev. Appl. **11**, 044047 (2019).

[71] O. Köksal and R. Pentcheva, Chern and Z_2 topological insulating phases in perovskite-derived 4*d* and 5*d* oxide buckled honeycomb lattices, Sci. Rep. **9**, 17306 (2019).

[72] B. Geisler, S. Follmann, and R. Pentcheva, Oxygen vacancy formation and electronic reconstruction in strained $LaNiO_3$ and $LaNiO_3/LaAlO_3$ superlattices, Phys. Rev. B **106**, 155139 (2022).

[73] See Supplemental Material at http://link.aps.org/supplemental/10.1103/PhysRevB.108.224502 for a direct comparison of the $NdNiO_2/KTaO_3$(001) interface electronic structure to that of the pristine $KTaO_3$(001) surface and an assessment of the Hubbard-U dependence of the key results.

[74] G. A. Sawatzky, Superconductivity seen in a non-magnetic nickel oxide, Nature (London) **572**, 592 (2019).

[75] H. J. Monkhorst and J. D. Pack, Special points for Brillouin-zone integrations, Phys. Rev. B **13**, 5188 (1976).

[76] Z. Zhang, S. Soltan, H. Schmid, H.-U. Habermeier, B. Keimer, and U. Kaiser, Revealing the atomic and electronic structure of a $SrTiO_3/LaNiO_3/SrTiO_3$ heterostructure interface, J. Appl. Phys. **115**, 103519 (2014).

[77] J. Hwang, J. Son, J. Y. Zhang, A. Janotti, C. G. Van de Walle, and S. Stemmer, Structural origins of the properties of rare earth nickelate superlattices, Phys. Rev. B **87**, 060101(R) (2013).

[78] S. H. Wemple, Some transport properties of oxygen-deficient single-crystal potassium tantalate ($KTaO_3$), Phys. Rev. **137**, A1575 (1965).

[79] U. T. Höchli, H. E. Weibel, and L. A. Boatner, Quantum limit of ferroelectric phase transitions in $KTa_{1-x}Nb_xO_3$, Phys. Rev. Lett. **39**, 1158 (1977).

[80] G. Bihlmayer, Band structure from first-principles and relativistic effects, in *48th IFF Spring School 2017 Topological Matter - Topological Insulators, Skyrmions and Majoranas,* edited by S. Blügel, Y. Mokrousov, T. Schäpers, and Y. Ando (Forschungszentrum Jülich GmbH Zentralbibliothek, Jülich, 2017).

[81] A. Sahinovic, B. Geisler, and R. Pentcheva, Nature of the magnetic coupling in infinite-layer nickelates versus cuprates, Phys. Rev. Mater. **7**, 114803 (2023).

[82] Y. M. Koroteev, G. Bihlmayer, J. E. Gayone, E. V. Chulkov, S. Blügel, P. M. Echenique, and P. Hofmann, Strong spin-orbit splitting on Bi surfaces, Phys. Rev. Lett. **93**, 046403 (2004).

[83] M. Kepenekian, R. Robles, C. Katan, D. Sapori, L. Pedesseau, and J. Even, Rashba and Dresselhaus effects in hybrid organic–inorganic perovskites: From basics to devices, ACS Nano **9**, 11557 (2015).

[84] X. Wu, K. Jiang, D. Di Sante, W. Hanke, A. P. Schnyder, J. Hu, and R. Thomale, Surface *s*-wave superconductivity for oxide-terminated infinite-layer nickelates, arXiv:2008.06009.

[85] L. P. Gor'kov and E. I. Rashba, Superconducting 2D system with lifted spin degeneracy: Mixed singlet-triplet state, Phys. Rev. Lett. **87**, 037004 (2001).

[86] A. Kreisel, Y. Quan, and P. J. Hirschfeld, Spin-triplet superconductivity driven by finite-momentum spin fluctuations, Phys. Rev. B **105**, 104507 (2022).

[87] R. Hakuno, K. Nogaki, and Y. Yanase, Magnetism and superconductivity in mixed-dimensional periodic Anderson model for UTe_2, arXiv:2306.00405.

[88] Z. Li and S. G. Louie, Two-gap superconductivity and decisive role of rare-earth *d* electrons in infinite-layer nickelates, arXiv:2210.12819.

[89] A. Chubukov and P. J. Hirschfeld, Iron-based superconductors, seven years later, Phys. Today **68**, 46 (2015).

[90] I. M. Lifshitz, Anomalies of electron characteristics of a metal in the high pressure region, Sov. Phys. JETP **11**, 1130 (1960).

[91] Y. Zhong, Z. Chen, S.-D. Chen, K.-J. Xu, M. Hashimoto, Y. He, S. ichi Uchida, D. Lu, S.-K. Mo, and Z.-X. Shen, Differentiated roles of Lifshitz transition on thermodynamics and supercon-

ductivity in $La_{2-x}Sr_xCuO_4$, Proc. Natl. Acad. Sci. USA **119**, e2204630119 (2022).

[92] M. Altmeyer, H. O. Jeschke, O. Hijano-Cubelos, C. Martins, F. Lechermann, K. Koepernik, A. F. Santander-Syro, M. J. Rozenberg, R. Valentí, and M. Gabay, Magnetism, spin texture, and in-gap states: Atomic specialization at the surface of oxygen-deficient $SrTiO_3$, Phys. Rev. Lett. **116**, 157203 (2016).

[93] M.-Y. Choi, K.-W. Lee, and W. E. Pickett, Role of $4f$ states in infinite-layer $NdNiO_2$, Phys. Rev. B **101**, 020503(R) (2020).